Physica D 70 (1994) 165–177
North-Holland

SSDI 0167-2789(93)E0277-I

PHYSICA D

Spatio–temporal dynamics in twin-stripe semiconductor lasers

O. Hess and E. Schöll

Institut für theoretische Physik, Technische Universität Berlin, Hardenbergstraße 36, D-1000 Berlin 12, Germany

Received 20 December 1992
Revised manuscript received 26 May 1993
Accepted 16 August 1993
Communicated by F.H. Busse

The twin-stripe semiconductor laser, a system of two evanescently coupled nonlinear oscillators, shows complex spatio–temporal behaviour. Its dynamics is studied theoretically by numerical integration of a model system of coupled partial differential equations. The overlap of the evanescent optical fields and the diffusion of charge carriers determine the amount of nonlinear transverse coupling between the laser stripes. The concept of cumulants of the bit–number of a dynamical system composed of two sub-systems, and a characteristic spatio–temporal correlation function are introduced and applied to quantify the complexities in space and time as they are observed in the output signal of the twin-stripe laser. Depending on the distance between the adjacent oscillators, three dynamical regimes are identified: Sufficiently far apart, the two laser oscillators are uncoupled and the device shows a steady constant output signal. In the regime of medium coupling, randomly oscillating light pulses dominate the output signal. If both stripes are strongly coupled, both lasers oscillate with a (fixed) phase lag but chaotic intensities.

1. Introduction

In a twin-stripe semiconductor laser, two laser stripes, each by itself representing a nonlinear oscillator, are combined to one single device. Being the simplest model system for a multi-stripe laser configuration which shows interaction between adjacent semiconductor laser oscillators, the twin-stripe laser also has technological significance. Examples are applications as directional couplers or optical amplifiers. Driven below its laser threshold, the twin-stripe laser represents an amplifier configuration which is widely employed in optical communication systems. Depending how far apart the two stripes are placed on the laser device, the oscillators of the twin-stripe laser are weakly or strongly coupled. Physically, the coupling is provided by the overlapping evanescent optical fields and by diffusion of charge carriers. It can range from the case of quasi-isolated independently operating laser to that of strongly coupled nonlinear oscillators.

In this paper the dynamic behaviour of the twin-stripe semiconductor laser is studied numerically in the framework of a continuous-time, continuous-space model [1] of coupled partial differential equations for the counterpropagating complex optical fields E^+ and E^- and the density N of electron–hole pairs in the active semiconductor laser medium. In contrast to previous studies of semiconductor laser array dynamics which were mostly based on models involving coupled mode theory [2], i.e. ordinary differential equations, numerical integration of our system of partial differential equations provides full information of the space and time dependence of the dynamical variables in the twin-stripe laser, i.e. the optical field and the carrier density. If required, especially for comparison with experimental results, data may then be either conveniently reduced by projection,

sampling of relevant information, or by spatial or temporal averaging.

This article is organized as follows: The following section 2 gives an outline of the model system of equations which describe the dynamical behaviour of the twin-stripe semiconductor laser and were introduced in [1]. In section 3 the dynamics of the twin-stripe waveguide laser is studied by numerically integrating the model system of coupled partial differential equations. The coupling-strength between the two laser stripes is changed by varying the interelement distance. With increasing coupling the dynamic behaviour of the twin-stripe laser shows a sharp transition from quasi-independently operating continuous wave ("cw") lasers to spatio–temporal chaos in the near-field output intensity. The concept of cumulants of the bit-number [3] is applied to the twin-stripe laser in section 4, and is used to characterize the variation of the twin-stripe output signal in time, highlighting the symmetry breaking transition which occurs in the laser with sufficiently strong interelement coupling. In section 5 we analyse the spatio–temporal correlations in the optical signal resulting from the nonlinear interaction between the two laser stripes. Section 6 draws some conclusions.

2. The semiconductor laser array model

Twin-stripe semiconductor lasers typically consist of an active layer of GaAs sandwiched between the cladding layers of $Al_xGa_{1-x}As$. One of the cladding layers may have a ribbed transverse structure as schematically shown in fig. 1.

If current is injected through the two current stripes on the top of the laser device, the active laser medium is locally excited, and with sufficient pumping, i.e. sufficiently high injection-current, the inversion-condition for laser operation is met. Light, created through interband recombination of electron–hole pairs, propagates in the cavity in longitudinal (z) direction and is partially reflected and partially transmitted

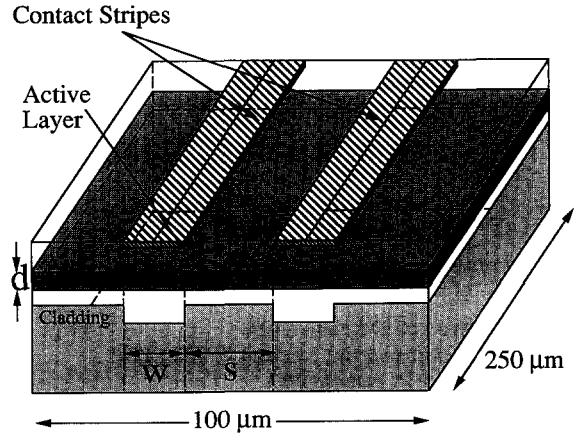

Fig. 1. Schematic structure of a combined gain- and index-guided twin-stripe laser. The active GaAs layer (shaded dark) is sandwiched between 2 cladding layers of $Al_xGa_{1-x}As$ (white). Charge carriers, injected through the two contact stripes at the top of the device (hatched) may recombine in the active zone. Light propagates in longitudinal (z) direction. The transverse ribbed cladding structure at the bottom serves as a passive waveguide. The transverse width w of the ribs and of the current stripes are generally chosen such that one stripe supports one transverse mode.

at the cleaved facets of the semiconductor laser structure. Due to the difference in optical properties of the individual layers and the transverse ribs, the semiconductor laser structure acts as a vertical (y-direction) and transverse (x-direction) optical waveguide for the light field in the cavity.

The transverse width w of the current stripes and the ribs of the cladding layer is chosen such that one stripe supports one transverse waveguide mode only. Strong waveguiding in the vertical (y) dimension effectively reduces the relevant spatial degrees of freedom for the counterpropagating optical fields and the electron–hole density to two. Parameters which account for the strong lateral waveguiding effects can be obtained from a steady-state analysis of the optical waveguiding properties of the layered structure. However, the optical properties in transverse and longitudinal direction are strongly influenced by local optical field and charge carrier properties and have to be determined self-consistently along with the aforementioned dynamic variables.

The theoretical description of the spatio-temporal behaviour of multi-stripe semiconductor lasers is based upon Maxwell's wave equation for the electric field $\boldsymbol{E}$

$$\left(\nabla^2 - \text{grad div} - \frac{1}{c^2}\frac{\partial^2}{\partial t^2}\right)\boldsymbol{E}(\boldsymbol{r}, t) = \frac{1}{\varepsilon_0 c^2}\frac{\partial^2}{\partial t^2}\boldsymbol{P}(\boldsymbol{r}, t)\,, \tag{1}$$

together with the appropriate material equations for the polarization $\boldsymbol{P}$ and the electron–hole density N, where c is the vacuum velocity of light and ε_0 is the absolute permittivity. Rapid decay of the polarization field in an excited semiconductor – which has been measured to be of the order of 50 fs [5] – justifies adiabatic elimination of the polarization $\boldsymbol{P}$ as a dynamic variable from the generalised semiconductor optical Bloch equations [6]. The polarization

$$\boldsymbol{P} = \varepsilon_0 \chi(N)\,\boldsymbol{E}\,, \tag{2}$$

with the optical susceptibility

$$\chi = \chi_0 + \chi_{n_\ell}(N) \tag{3}$$

$$= \chi' + \mathrm{i}\chi''\,, \tag{4}$$

is conveniently expressed in terms of the (complex) linear part χ_0 and the (complex) contribution χ_{n_ℓ} which depends on the charge carrier density N. Alternatively, χ is split into its real (χ') and imaginary (χ'') parts. Moreover, it is assumed that the optical field and the polarization are linearly polarized perpendicular to the z-axis. The optical field propagates in longitudinal z-direction. Performing the paraxial ray approximation, i.e. separating the optical field variables into longitudinally slowly varying counterpropagating optical fields E^+ and E^- while considering fast transverse dynamics according to

$$E(x, z, t) = \tfrac{1}{2}E^+(x, z, t)\exp(\mathrm{i}k_z z - \mathrm{i}\omega t) + \tfrac{1}{2}E^-(x, z, t)\exp(-\mathrm{i}k_z z - \mathrm{i}\omega t) + \text{c.c.}\,, \tag{5}$$

where $k_z = n_\ell k_0$ includes k_0, the optical wavenumber in vacuum and $n_\ell = \mathrm{Re}(\sqrt{1+\chi_0})$ the refractive index of the active layer, where Re indicates the real part. The optical frequency is denoted by ω. After appropriate scaling, follows the system of coupled nonlinear partial differential equations [1, 9]

$$\frac{\partial E^+}{\partial z} + \frac{n_\ell}{c}\frac{\partial E^+}{\partial t} = \mathrm{i}D_\mathrm{p}\frac{\partial^2 E^+}{\partial x^2} - \mathrm{i}\mathcal{W}(x)\,E^+ + \Gamma(x)[g(N) - \mathrm{i}\alpha a N]E^+\,, \tag{6}$$

$$-\frac{\partial E^-}{\partial z} + \frac{n_\ell}{c}\frac{\partial E^-}{\partial t} = \mathrm{i}D_\mathrm{p}\frac{\partial^2 E^-}{\partial x^2} - \mathrm{i}\mathcal{W}(x)\,E^- + \Gamma(x)[g(N) - \mathrm{i}\alpha a N]E^-\,, \tag{7}$$

$$\frac{\partial N}{\partial t} = D_\mathrm{f}\frac{\partial^2 N}{\partial x^2} + \Lambda(x) - \frac{N}{\tau} - g(N)(|E^+|^2 + |E^-|^2)\,. \tag{8}$$

Excitation of the active semiconductor medium is provided through the injection of charge carriers, represented by the transversely dependent pumping term

$$\Lambda(x) = \begin{cases} j\dfrac{\eta}{ed}\,, & x_i - \tfrac{1}{2}w \leqslant x \leqslant x_i + \tfrac{1}{2}w\,, \\ 0\,, & \text{otherwise}\,, \end{cases} \tag{9}$$

where $x_i, i = 1, 2$ is the center of the ith laser stripe and w its width. The injection current density is denoted by j, and η represents the injection efficiency, i.e. the proportion of carriers which actually reaches the active region; e is the charge of an electron and d the (vertical) thickness of the layer. In the phenomenological representation adopted here one thinks of the semiconductor gain medium as being homogeneously broadened. The gain g, describing the interaction of light with matter, and the refractive index are regarded independent of wavelength. The gain g and the change of the refractive index δn of the active medium which is due to the injection of charge carriers are assumed

linearly dependent on the dynamic carrier density N and modelled by the gain-function

$$g(N) = a(N - N_0) = \frac{\omega}{n_\ell^2}\chi''(N) \tag{10}$$

and

$$\delta n = -\frac{1}{k_0}\alpha a N = \frac{1}{n_\ell \epsilon_0}\chi'_{n_\ell}, \tag{11}$$

respectively. The differential gain is denoted by a and N_0 is the carrier density at transparency. The linewidth enhancement factor $\alpha = (\partial\chi'/\partial N)/(\partial\chi''/\partial N)$ is assumed constant, i.e. spatial and temporal variations of α are disregarded. Generally, the values of α range from 2 to 6 in the case of GaAs/Al_xGa_{1-x}As bulk semiconductor lasers. The diffraction coefficient $D_p = (2n_\ell k_0)^{-1}$ includes the index of refraction n_ℓ and the wavenumber k_0, where the space dependence of the refractive index through $N(x)$ has been neglected. The influence of transverse variations of N on the diffusion coefficient D_f is also disregarded. The nonradiative decay of the electron–hole density is represented by the relaxation time τ. The transverse passive waveguiding properties, resulting from the difference in refractive index between the layers of different semiconductor material or differently doped regions of the sandwich-like laser structure, are characterized by

$$\mathcal{W}(x) = \begin{cases} k_0(n_c - n_{eff}), & x_i - \frac{1}{2}w \leq x \leq x_i + \frac{1}{2}w, \\ k_0 n_c, & \text{otherwise}. \end{cases} \tag{12}$$

In the spirit of the effective index approximation [7], the effective index n_{eff} has been obtained from an analysis in the steady state together with the confinement factor

$$\Gamma(x) = \begin{cases} 0.5149, & x_i - \frac{1}{2}w \leq x \leq x_i + \frac{1}{2}w, \\ 0.5013, & \text{otherwise}, \end{cases} \tag{13}$$

which represents the transverse dependence of the vertical confinement of the optical field to the active layer.

Together with the relevant *longitudinal* boundary conditions

$$E^+(x, z = 0, t) = -\sqrt{R_1}\, E^-(x, z = 0, t), \tag{14}$$

$$E^-(x, z = L, t) = -\sqrt{R_1}\, E^+(x, z = L, t), \tag{15}$$

which represent reflection of the optical fields at the facet mirrors $z = 0$ and $z = L$ of the laser structure and the *transverse* boundary conditions

$$\frac{\partial E^\pm}{\partial x} = -\alpha_w E^\pm \quad \text{and} \quad \frac{\partial N}{\partial x} = -\tilde{v}_{sr} N \quad \text{at } x = +\tfrac{1}{2}w, \tag{16}$$

$$\frac{\partial E^\pm}{\partial x} = +\alpha_w E^\pm \quad \text{and} \quad \frac{\partial N}{\partial x} = +\tilde{v}_{sr} N \quad \text{at } x = -\tfrac{1}{2}w, \tag{17}$$

accounting for the strong absorption of the optical fields (constant α_w) in the "wings" outside the laser stripes and surface recombination effects of the charge carriers, eqs. (6)–(8) constitute the model equations which are the basis for our theoretical and numerical investigation of the dynamics of the twin-stripe laser. Note that the surface recombination-coefficient $\tilde{v}_{sr} = s/D_f$ includes the surface recombination velocity s and the transverse diffusion-coefficient D_f [8]. Typical physical parameter values used in the computations are listed in table 1.

3. Dynamics of the twin-stripe laser

The coupled system of nonlinear partial differential equations is solved by discretizing eqs. (6)–(8) in time (t) and space (x, z). The resulting finite-difference equations are integrated using the *Hopscotch* method [1,9,14].

The dynamic variables in the twin-stripe laser in (6)–(8) are the charge carrier density N and the counterpropagating optical fields E^+ and E^-. Experimentally most detectors generally measure the intensity ($I \sim |E^\pm|^2$). Consequently N and I are considered as dynamic variables, although in the simulations, $E^\pm$, which include

Table 1
Numerical parameters used in the computations.

L (cavity length)	250 μm
d (thickness of active layer)	0.15 μm
w (stripe width)	5 μm
R_1, R_2 (mirror reflectivities)	0.32, 0.99
n_e(refractive index of active layer)	3.59
n_c (refractive index of cladding)	3.35
n_{eff} (effective index)	3.42
α (linewidth enhancement factor)	2
a (gain coefficient)	1.5×10^{-16} cm^2
N_0 (transparency concentration)	0.67×10^{18} cm^{-3}
λ (laser wavelength)	815 nm
D_f (diffusion coefficient)	30 cm^2/s
D_p (diffraction coefficient)	18×10^{-6} m
τ (nonradiative recombination time)	5 ns
η (injection efficiency)	0.5
J (injection current)	100 mA
α_w (absorption in the "wings")	30 cm^{-1}
s (surface recombination velocity)	10^6 m/s
Γ (confinement factor)	0.5013/0.5149 (within/outside the ridge)

vital phase information, are computed. At the start of the simulations at $t = 0$, the real parts of the optical fields $E^{\pm}$ are initialized with very small ($\sim 10^{-6}$ in dimensionless units) random values; the imaginary part is initialized with zero. The density N is initialized homogeneously with small values and the injection current $J(x)$ is switched on with a step-function at $t = 0$.

Important device parameters for the twin-stripe laser configuration are the actual separation s of the two laser stripes (fig. 1), their width w, thickness of the active layer d, the length of the device L and the amount of coupling-out at the facets, represented by the mirror reflectivities R_1 and R_2. Externally the device can be driven, and to a certain extend controlled, by the amount of pumping in the form of injected charge carriers, i.e. by the injection current J. If J is chosen below the cw laser threshold value J_{th}, the twin-stripe laser can be used as an amplifier for optical signals, rather than as a light generating device. On the other hand, the higher $J > J_{th}$ is chosen, the faster the relaxation oscillations are which every semiconductor laser displays before assuming a steady state output signal [10]. However, due to ohmic losses, very high injection current values lead to strong heating effects which are not included in the model presented here.

In the simulations a moderate and fixed injection current $J = jLw = 100$ mA is chosen – about twice the threshold current of the twin-stripe laser. Rather the interelement distance s between the two laser stripes, being the prominent coupling parameter between the two nonlinear laser-oscillators of the twin-stripe laser, is varied. It is changed in the regime between 5 μm and 16 μm and all other parameters are held constant.

In fig. 2 the time dependence of the trans-

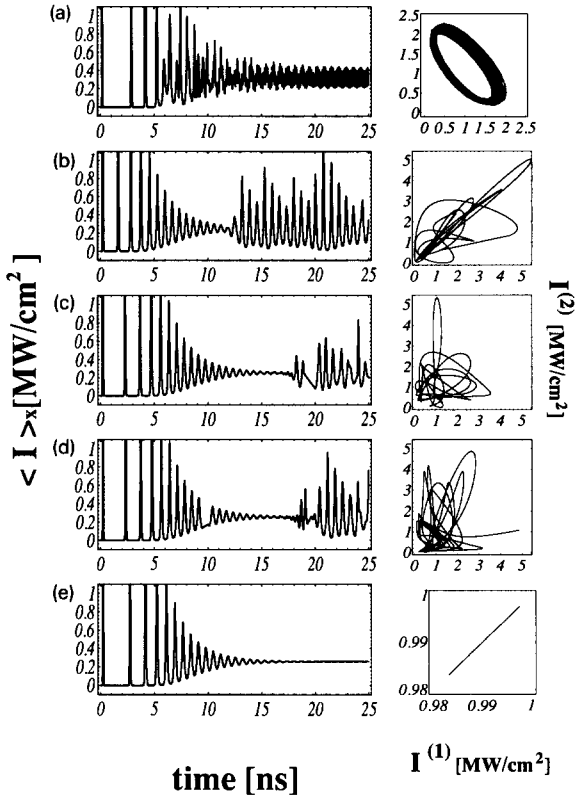

Fig. 2. Time dependence of the transversely averaged output intensity (left column) and phase-portrait of the output intensity at the center of laser stripe 2 ($I^{(2)}$) versus that of laser stripe 1 ($I^{(1)}$) (right column) for various stripe separations: $s = 5$ μm (a), 10 μm (b), 12 μm (c), 13 μm (d) and 14 μm (e). The numerical parameters are given in table 1.

versely averaged output intensity $\langle I \rangle_x$, with $I(x,t) = T_1/Z|E^-(x, z=0, t)|^2$, $Z = n_e/(\varepsilon_0 c)$ and $T_1 = 1 - R_1$ being the optical wave-resistance in the semiconductor medium and the transmittivity of the front mirror, respectively, i.e. the signal as measured by a large detector in front of the laser, is shown for various values of the stripe separation s. The corresponding phase portraits of the output signals at the center position of each stripe $I^{(2)}$ versus $I^{(1)}$ show the dynamical behaviour of the two stripes during the time interval from 20 to 25 ns. At the largest stripe separation $s = 14$ μm (fig. 2e)) either laser stripe behaves "as if the other one would not be there" and individually shows relaxation oscillations (*spiking*) typical for semiconductor lasers: after initial spikes in the output signal, each individual laser stripe and thus the output intensity of the whole device relaxes to its stable steady state operating value. Being identical in their transverse width, passive optical properties and subject to the same amount of pumping, stripe 1 and 2, which have almost identical initial conditions at the start of the computation, oscillate synchronously, as can be seen in the corresponding phase portraits of their respective output intensities $I^{(2)}$ versus $I^{(1)}$. The coupling between the stripes is sufficiently weak so that their own "generic" oscillations which are thus expected to be very similar are unaffected by the mutual interaction and the laser-stripes are quasi-decoupled. However, if the distance between the two stripes is only slightly smaller, the coupling between them, provided by the overlap of the evanescent optical fields and the diffusion of charge carriers, is sufficiently strong so that the behaviour of each individual stripe and also that of the whole device is changed dramatically. In fig. 2d the two laser stripes are separated by 13 μm. Initially the twin-stripe laser shows relaxation oscillations similar to those observed in the case of $s = 14$ μm, but after about 15 ns the two laser stripes no longer oscillate in phase with each other and start to pulsate chaotically. This is indicated in the plot of the transversely averaged output signal as well as in the phase portrait of both individual laser stripes. This behaviour is augmented when s is further reduced (figs. 2a–d). At the minimum stripe separation $s = 5$ μm, which equals the width w of one stripe, the coupling between the two stripes is sufficiently strong to cause high-frequency alternating oscillations of the two stripes.

Thus at very strong interelement coupling the twin-stripe laser oscillates on a narrow chaotic band reminiscent of a smeared-out limit cycle (fig. 2a). The smearing-out appears to indicate some loss of spatial coherence of subsequent oscillations. In the case of "medium" coupling at stripe separations $10\ \mu\text{m} \lesssim s \lesssim 13\ \mu\text{m}$ the output signal pulsates randomly with considerably higher spikes than in the case of very strong coupling. Finally when both stripes are sufficiently far from each other both laser oscillators are decoupled, and oscillate independently; thus the device shows a stable continuous-wave output signal (see figs. 2e, 3f, respectively).

Intensity-plots extracted from the simulation data provide a direct impression of the spatio–temporal dynamics of the twin-stripe laser array, as it would be measured at one facet of the laser. Such plots of the time interval from 20 to 25 ns (i.e., post spiking period) shown in fig. 3 visualize the unstable behaviour of the twin-stripe laser output when both stripes are sufficiently close. Dark colours indicate low intensity and bright colours represent high output intensities. The high-frequency regularly alternating oscillations in the strong-coupling limit (fig. 3a), the chaotically blinking oscillations in the medium-coupling regime (figs. 3b–e) and the quasi-cw oscillations in the low-coupling limit (fig. 3f) are clearly visible.

Although directly monitoring the phase of the optical field in the laser is not possible experimentally, our numerical simulation procedure (using complex optical fields) can easily provide it. The dynamics of the twin-stripe laser is vividly highlighted in jointly considering the optical output signals $I^{(1)}$ and $I^{(2)}$ of laser stripes

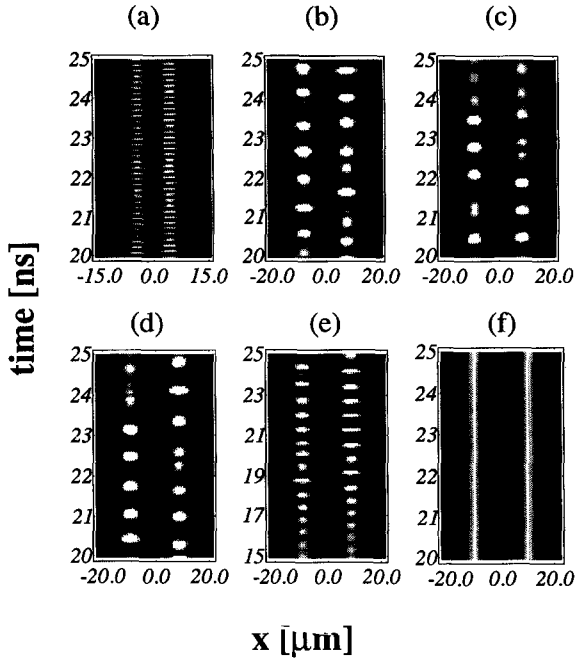

Fig. 3. Near-field intensity plots in the x (transverse coordinate)–time plane as obtained at one facet of the laser structure. Bright colours represent high light intensity, dark shading indicates low intensity values. Stripe separations: $s = 5$ μm (a), 10 μm (b), 11 μm (c), 12 μm (d), 13 μm (e) and 14 μm (f).

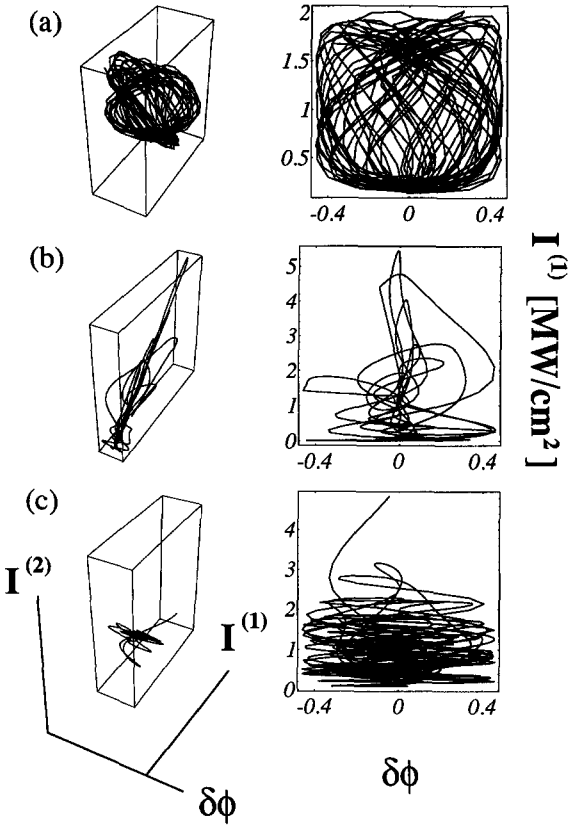

Fig. 4. Phase-space representation of the optical output signals $I^{(1)}$ and $I^{(2)}$ of laser stripes 1 and 2, respectively, and the phase difference $\delta\phi$ of the respective optical fields (left column). The right column shows the projection onto the $(I^{(1)}, \delta\phi)$ phase plane. The time interval is from 20 to 25 ns. Stripe separations: $s = 5$ μm (a), 11 μm (b), 13 μm (c).

1 and 2, respectively, and the phase-difference $\delta\phi$ of the respective optical fields in a phase-space representation which is presented in fig. 4 (left column). Three examples from a twin-stripe laser with moderately and strongly coupled laser stripes are chosen with stripe separations of $s =$ 5 μm (a), 11 μm (b) and 13 μm (c). The corresponding projection onto the $(\delta\phi, I^{(1)})$ phase plane is shown in the right column of fig. 4. In the case of $s = 14$ μm, which is not shown, the phase difference $\delta\phi$ vanishes and the three-dimensional $(I^{(1)}, I^{(2)}, \delta\phi)$ representation (left column of fig. 4) reduces to the one in fig. 2e. Hence in this case both laser stripes oscillate completely in phase. However, with only slightly smaller stripe separation at $s = 13$ μm the phase difference between the two stripes exhibits chaotic oscillations (fig. 4c).

In the regime of medium coupling where the output signal of the twin-stripe laser shows intense random pulsations (figs. 2b, c and figs. 3b–d) the trajectory in the $(I^{(1)}, I^{(2)}, \delta\phi)$ space and its projection onto the $(I^{(1)}, \delta\phi)$ plane (fig. 4b) show that the system suddenly experiences an abrupt kick through high-intensity bursts and subsequently spirals back on a submanifold in phase space at smaller values of $I^{(1)}$ and $I^{(2)}$. This screw-type reinjection of the trajectory is reminiscent of Shilnikov chaos, which has recently been found in coupled nonlinear oscillator systems [11].

Finally, at very strong coupling between the two laser stripes at a stripe separation of $s =$

5 μm (fig. 4a) the optical output signals $I^{(1)}$ and $I^{(2)}$ of the twin-stripe laser oscillate chaotically within a narrow intensity band around the steady state of the uncoupled laser with a strongly oscillating phase difference $\delta\phi$.

4. Cumulants of the bit-number

In the context of nonequilibrium phase transitions *Schlögl* [12, 13] suggested to use cumulants of the bit-number $b = -\ln \rho$ of a probability distribution ρ to characterize systems far from thermodynamical equilibrium. The bit-number cumulants C_k of order k are defined by the power series expansion of the generating function

$$\ln\langle \exp \eta b \rangle = \sum_{k=1}^{\infty} C_k \frac{\eta^k}{k!}, \tag{18}$$

with the mean value given by $\langle a \rangle = \int \mathrm{d}x\, \rho(x)\, a(x)$. The first cumulants $C_1 = \langle b \rangle$ and $C_2 = \langle b^2 \rangle - \langle b \rangle^2$ are the *Shannon* information entropy and the bit-number variance, respectively. The bit-number cumulants in particular the variance, of the asymptotic invariant density $\rho(x) = \lim_{T\to\infty} T^{-1} \int_0^T \mathrm{d}t\, \delta(x - x(t))$ of a nonlinear dynamic flow $x(t)$ were introduced as characteristic critical measures of chaotic dynamical systems [3]. To a higher degree than the *Shannon* information entropy the bit-number variance is sensitive to correlations between subsystems [3,4]. Moreover, the latter represents a meaningful correlation measure not only for linear correlations where the linear correlation factor appears to be an appropriate measure but also for *nonlinear* correlations [4].

Here the bit-number variance of the asymptotic invariant density of the dynamical system is proposed as a correlation measure to characterize the dynamics of the twin-stripe laser. Individually both laser-stripes can be regarded as sub-systems of the whole dynamical system (i.e. the twin-stripe laser), each laser-stripe nonlinearly coupled to the other one. Besides the intensities $I^{(1)}$ and $I^{(2)}$, the respective values of the carrier densities $N^{(1)}$ and $N^{(2)}$ in the center of stripes 1 and 2 constitute the phase-space considered for the twin-stripe laser. The subspace $(I^{(1)}, I^{(2)})$ of the phase space $(I^{(1)}, N^{(1)}, I^{(2)}, N^{(2)})$ is partitioned into $M \times M$ cubic boxes of length ϵ. The signal intensities $I^{(1)}$ and $I^{(2)}$ are monitored at intervals of time Δt. The phase-values $\phi^{(1)}$ and $\phi^{(2)}$ of the respective optical fields span a phase-space analogous to the field intensities and, although specifically formulated for $I^{(1)}$ and $I^{(2)}$, the equations and comments below also apply to $\phi^{(1)}$ and $\phi^{(2)}$.

Let p_{ij} be the joint probability that $I^{(1)}$ lies in the ith and $I^{(2)}$ in the jth box of the phase-space partition. The bit-number cumulants C_1 and C_2 are then obtained according to

$$C_1 = -\sum_{i,j} p_{i,j} \cdot \ln p_{i,j}, \tag{19}$$

$$C_2 = \sum_{i,j} p_{i,j} \cdot (\ln p_{i,j})^2 - \left(\sum_{i,j} p_{i,j} \cdot \ln p_{i,j}\right)^2. \tag{20}$$

In the case of uncorrelated subsystems where the two laser stripes oscillate without correlation, the joint probability can be factorized as

$$p_{i,j} = p_i^{(1)} \cdot p_j^{(2)} \tag{21}$$

$$= \left(\sum_j p_{ij}\right) \cdot \left(\sum_i p_{ij}\right) \tag{22}$$

and the uncorrelated cumulants are additive

$$C_1^0 = C_1^{(1)} + C_1^{(2)}, \tag{23}$$

$$C_2^0 = C_2^{(1)} + C_2^{(2)}, \tag{24}$$

with

$$C_1^{(k)} = -\sum_l p_l^{(k)} \cdot \ln p_l^{(k)}, \tag{25}$$

$$C_2^{(k)} = \sum_l p_l^{(k)} \cdot (\ln p_l^{(k)})^2 - \left(\sum_l p_l^{(k)} \cdot \ln p_l^{(k)}\right)^2 . \tag{26}$$

For convenience the correlation between the two lasers is considered in the following in terms of the normalized cumulants:

$$\delta C_1 = (C_1^0 - C_1)/C_1^0 , \tag{27}$$

$$\delta C_2 = (C_2^0 - C_2)/C_2^0 , \tag{28}$$

which are zero for uncorrelated subsystems, and increase with *growing* correlation. For complete *linear* correlation, i.e. $p_{ij} = p_i^{(1)}\ \delta_{ij} = p_j^{(2)}\delta_{ij}$, one obtains $C_1 = C_1^{(1)} = C_1^{(2)} = \frac{1}{2}C_1^0$ and $C_2 = C_2^{(1)} = C_2^{(2)} = \frac{1}{2}C_2^0$, and hence $\delta C_1 = \delta C_2 = 0.5$, provided that $C_1^0, C_2^0 \neq 0$.

In fig. 5 the normalized cumulants δC_1 and δC_2 of the intensities $I^{(1)}, I^{(2)}$ in the time interval from 20 to 50 ns with $\Delta t = 8.33 \cdot 10^{-3}$ ns (see fig. 2) are plotted. Both δC_1 and, in a more pronounced way, δC_2 show a sharp increase between $s = 13$ μm and $s = 14$ μm which corresponds to the symmetry-breaking transition from the randomly oscillating twin-stripe laser at $s = 13$ μm to the situation of $s = 14$ μm where both laser stripes exhibit transient relaxation oscillations with fixed phase relation before approaching the symmetric fixed point. Note that the numerically calculated bit-number cumulants converge very slowly with increasing number of

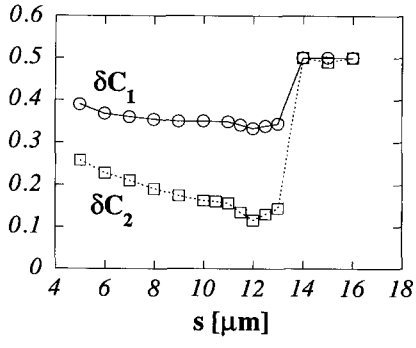

Fig. 5. Normalized bit-number cumulants δC_1 and δC_2 of the intensity I of the twin-stripe laser as a function of the stripe separation s ($M = 400$, $\Delta t = 8.33 \times 10^{-3}$ ns).

data points N due to transients, and the numerical values C_i^{num} differ from the theoretical values C_i by

$$C_i^{\text{num}} = C_i + N_0 \frac{(\ln N)^i}{N} + \mathcal{O}\left(\frac{\ln N^{i-1}}{N}\right), \tag{29}$$

where N_0 is the number of data points which are not contained in a box covering the attractor. Therefore all calculated values are expected to decrease further if longer time series are used.

For $s \geq 14$ μm, $I^{(1)}$ and $I^{(2)}$ are fully linearly correlated, due to the symmetrically chosen initial conditions, leading to $\delta C_1 = \delta C_2 = 0.5$.

For more realistic, asymmetric initial conditions, this sharp transition between uncorrelated turbulent oscillations and regular relaxation oscillations with fixed phase lag is still retained since δC_i differs from 0.5 only to the order of $1/M$. Note that the apparent correlation for $s \geq 14$ μm is a result of the temporal coherence of each individual laser and *not* a measure of their coupling. Note further that in this case the bit-number cumulants are determined by the *transient* relaxation oscillations, rather than by the *asymptotic* invariant density, since the latter corresponds to a fixed point, giving vanishing cumulants C_1, C_1^0, C_2, C_2^0, and hence undefined δC_1, δC_2.

The bit-number variance δC_2 has a more distinct structure than δC_1, and assumes its smallest values around $s = 12$ μm. The increase of δC_2 for s decreasing from $s = 12$ μm to $s = 5$ μm indicates the onset of correlations in the regime of strongly coupled laser stripes with small stripe separation even before this is visible in the phase portraits or intensity plots. The bit-number variance thus provides a sensitive quantitative measure of the spatio-temporal correlations.

In analogy to fig. 5, fig. 6 shows the normalized cumulants δC_1 and δC_2 of the optical phases $\phi^{(1)}, \phi^{(2)}$ of the two stripes as a function of the stripe separation s for the same time interval. The phase of the optical field in laser stripe 1 and laser stripe 2 oscillates in the GHz-regime and is

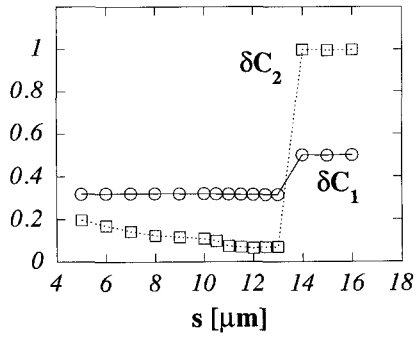

Fig. 6. Normalized information entropy δC_1 and normalized bit-number variance δC_2 of the phase ϕ of the optical field as a function of the stripe separation s of the twin-stripe laser ($M = 400$, $\Delta t = 8.33 \times 10^{-3}$ ns).

highly sensitive to correlations. The steep increase of δC_2 from almost zero to 1 between $s = 13$ μm and $s = 14$ μm signals the abrupt transition from uncorrelatedly oscillating laser stripes in the case of $s = 13$ μm to complete phase correlation between $\phi^{(1)}$ and $\phi^{(2)}$ at $s = 14$ μm. Note that in this case, due to linearly increasing, locked phases $\phi^{(k)} = \omega t$, $k = 1, 2$, the distribution $p_{ij} = p_i^{(1)}\ \delta_{ij} = p_j^{(2)}\delta_{ij}$ is an equipartition over n cells so that $C_1 = C_1^{(1)} = C_1^{(2)} = \frac{1}{2}C_1^0 = \ln n$, while $C_2 = C_2^{(1)} = C_2^{(2)} \equiv 0$, whence $\delta C_1 = 0.5$ but $\delta C_2 = 1$. It is remarkable that δC_1 remains constant over the whole range from $s = 13$ μm to $s = 5$ μm, whereas δC_2 slightly increases with decreasing s, demonstrating the greater sensitivity of the bit-number variance to correlations [3]. However, the increase of correlations is much more pronounced for the intensities than for the phase of the optical field.

5. Spatio-temporal correlations

As shown in section 3, the twin-stripe laser shows complex behavior in space and time (see fig. 3) under certain conditions. Depending on the actual interelement coupling the two laser stripes can oscillate independently but in phase, or show random pulsations in the output signal. The spatio-temporal correlation function

$$g(x_0, x, \tau) = \frac{\langle \delta I(x_0, t)\, \delta I(x, t+\tau)\rangle_t}{\sqrt{\langle \delta I^2(x_0, t)\rangle_t}\sqrt{\langle \delta I^2(x, t)\rangle_t}} \qquad (30)$$

is proposed as a measure to simultaneously quantify correlations in time and space which occur in the output signal of the twin-stripe laser. Above, $\langle \cdots \rangle_t$ is the average over time t and $I(x, t)$ is the field intensity at the laser facet at the transverse position x and $\delta I(x, t) = I(x, t) - \langle I(x, t)\rangle_t$ is the deviation of the intensity at the point x from its temporal average $\langle I(x, t)\rangle_t$. The correlation function g thus determines how much the output signal at the reference point x_0 and at the time t is correlated with the signal at the transverse position x at the time $t + \tau$.

Fig. 7 shows the spatio-temporal correlation function g for the time-interval from 20 to 50 ns and varying correlation time τ. The spatial reference point is placed in the center of the right laser stripe, i.e. $x_0 = x_2$. At strong interelement coupling at $s = 5$ μm, where the output signal shows high-frequency regular oscillations (see fig. 3a), the correlation function g (see fig. 7a) indicates that the output signal is strongly correlated across the whole width of the twin-stripe laser within a correlation time $\tau_{(a)} \approx 100$ ps. Note that the left laser stripe is strongly correlated to the right one (where the reference point x_0 has been placed). Successive correlation and anti-correlation maxima occur about every 100 to 200 ps, roughly corresponding to the time between two successive light pulses in each laser stripe. In the case of medium coupling, where the interelement separation is 11 μm and 13 μm (figs. 7b, c), the two output signals are considerably less spatially correlated with each other. Figs. 7b, c show that in space g is highest just around the reference point $x_0 = x_2$ and in time for small values of τ. However, the series of (irregular) light pulses from the left laser stripe ($x = -x_0$) still shows considerable correlation to the sequence emitted from the right one for small correlation times, followed by a depression in g. A next maximum in the correlation occurs after about 1 ns. Fig. 7d shows that in the case of

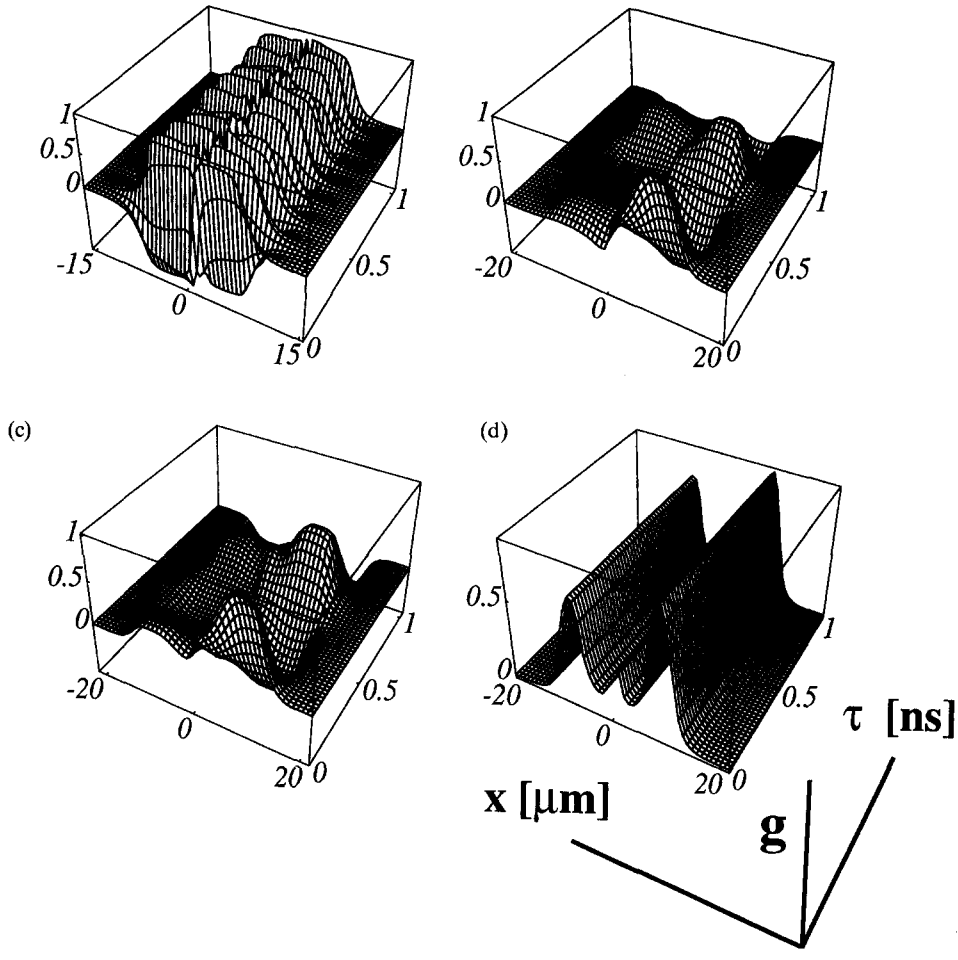

Fig. 7. Spatio–temporal correlation function g as a function of the transverse coordinate x and time delay τ with reference to the center of the right stripe. Stripe separations and spatial reference points: (a) $s = 5$ μm, $x_0 = 5$ μm; (b) $s = 11$ μm, $x_0 = 8$ μm; (c) $s = 13$ μm, $x_0 = 9$ μm; (d) $s = 14$ μm, $x_0 = 9.5$ μm. The time average is taken from $t = 20$ ns to $t = 50$ ns.

the quasi uncoupled laser stripes at $s = 14$ μm the correlation remains constant in τ. The highest correlation is to be found around the reference point $x_0 = x_2 = 9.5$ μm, and at $x = -x_0$, reflecting the cw operation of two identical lasers.

We define a measure of transverse complexity with the reference point x_0, by the maxima of g with respect to all delay times τ

$$G(x_0, x) = \underset{\tau}{\text{Max}}\, g(x_0, x, \tau)\,. \tag{31}$$

Choosing the reference point in the center x_1 of the laser stripe 1 (i.e. $x_0 = x_1$), the dependence of G on the transverse coordinate x for different stripe separations is shown in fig. 8. Compared to the correlation g in space and time, G does not reveal how quickly the transverse correlations decay. However, in showing the maximum correlation for all times τ, it gives a clear indication of how much the intensity signal at the center of the left laser stripe (x_0) is correlated with, say, the center of the right laser stripe, indicated by the second, smaller peak at $x = |x_0|$. Especially in the case of the strongly coupled twin-stripe laser (fig. 8a), G confirms the strong correlation between the oscillations of the two laser stripes. This correlation becomes successively smaller when the separation between the

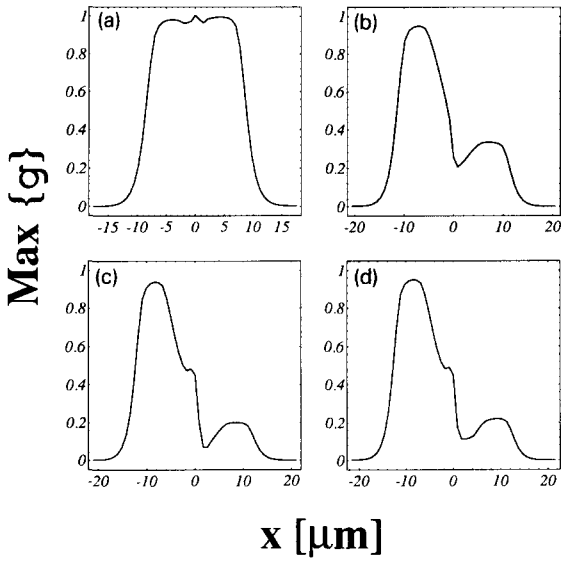

Fig. 8. Temporal maxima of the correlation function g versus x with reference to the center of the left stripe, $x_0 = -5$ μm (a), -8 μm (b), -8.5 μm (c), -9 μm (d). Stripe separations (left to right, top to bottom): $s = 5$ μm (a), 11 μm (b), 12 μm (c) and 13 μm (d). The time interval considered is from $t = 20$ ns to $t = 50$ ns.

oscillators is increased from 10 to 13 μm (figs. 8b–d).

6. Conclusion

We have investigated the dynamical behaviour of the two-stripe laser. On the basis of a model for semiconductor laser arrays outlined in section 2, numerical simulations of the system of coupled partial differential equations for the optical fields and the charge carrier density were performed and analysed.

It was shown (section 3) that the coupling of the overlapping evanescent optical fields in each laser stripe and the diffusion of carriers lead to complex spatio–temporal behaviour [15–17] if the two laser stripes are in sufficiently close vicinity to each other. This particular fact underlines the importance of our full spatio–temporal approach to the dynamics of the twin-stripe laser, as opposed to discrete coupled-oscillator models. In our simulations spatial and temporal degrees of freedom were fully taken into account and averaging techniques were only employed in the analysis of the data obtained from the simulation.

At an interelement separation s between 14 μm and 13 μm the output signal of the twin-stripe laser shows an abrupt symmetry breaking nonequilibrium phase transition and becomes unstable for smaller values of s. Varying the stripe-separation and thus the interelement coupling, the various regimes of spatio–temporal complexity in the output signal of the laser were analysed.

To this means the first two cumulants of the bit-number, viz. the information entropy and in particular the bit-number variance, on the one hand, and a characteristic spatio–temporal correlation function on the other hand, were employed for the quantification of the correlations between the subsystems constituted by the two laser stripes of the device. The bit-number variance of the intensity output turns out as a significant quantitative measure for the observed transition between strongly, moderately coupled and uncoupled oscillators. Correspondingly the dependence of the bit-number of the phase of the optical field on the stripe separation clearly shows that the two laser stripes oscillate with fixed phase when uncoupled in contrast to the strongly coupled case where all phase-coherence is lost with the output signal of the laser showing random pulsations.

Phase-portraits of the two output signals $I^{(1)}$ and $I^{(2)}$ together with the difference $\delta\phi$ of the phase of the optical field of laser stripe 1 and 2, respectively, identify three regimes: Indicated by oscillations in the phase difference $\delta\phi$, $I^{(1)}$ and $I^{(2)}$ oscillate out of phase around the steady state output signal of the corresponding uncoupled device in the case of strong coupling between the oscillators. In the other extreme case, with completely decoupled laser stripes, the phase difference remains constant and each laser stripe oscillates independently in a stable cw mode with

fixed phase. In the intermediate regime, with stripe separation $10\,\mu m \leq s \leq 13\,\mu m$ the twin-stripe laser shows complex spatio-temporal behaviour which is reminiscent of Shilnikov chaos: random pulsations in the output signal with sudden intensity bursts and chaotically oscillating phase difference between the stripes.

We suggest the following interpretation of our findings. For small separation, the strongly coupled laser stripes oscillate chaotically in a regime of weak turbulence. With increasing stripe separation the correlations between the two stripes gradually become weaker. This loss of spatial coherence increases the number of spatio-temporal degrees of freedom, thus enabling more complex spatio-temporal chaos indicative of strong turbulence. However, at a critical maximum stripe separation ($x \approx 14\,\mu m$) the spatial coupling is so weak that the nonlinear interaction between different localized degrees of freedom can no longer maintain a turbulent state. After an abrupt transition the two stripes behave as individual lasers each of which, due to its smaller number of degrees of freedom, exhibits a stable, more ordered (thus appearing more strongly correlated) state.

Acknowledgement

Partial financial support from the European Community is gratefully acknowledged. O.H. wants to thank J.V. Moloney for his stimulating influence. We thank H.-P. Herzel for valuable and interesting discussions. We are indebted to one of the referees for pointing out the logarithmic dependence of the bit-number cumulants upon the transients as the reason for their slow convergence.

References

[1] H. Adachihara, O. Hess, R. Indik and J.V. Moloney, Semiconductor laser array dynamics: numerical simulations on multi-stripe index-guided lasers, J. Opt. Soc. Am. B, 10 (1993) 496.

[2] S.S. Wang and H.G. Winful, Dynamics of phase-locked semiconductor laser arrays, Appl. Phys. Lett. 52 (1988) 1774–1776;
H.G. Winful and S.S. Wang, Stability of phase locking in coupled semiconductor laser arrays, Appl. Phys. Lett. 52 (1988) 1894–1896;
H.G. Winful and L. Rahman, Synchronized chaos and spatiotemporal chaos in arrays of coupled lasers, Phys. Rev. Lett. 65 (1990) 1575.

[3] F. Schlögl and E. Schöll, Generalized specific heat as a characteristic measure in chaos, Z. Phys. B 71 (1988) 231.

[4] H. Naber and E. Schöll, Bit-number cumulants as a correlation measure of self-generated oscillations in a semiconductor model for low-temperature impurity break-down, Z. Phys. B 78 (1990) 301.

[5] H. Haug and S.W. Koch, Semiconductor laser theory with many-body effects, Phys. Rev. A 39 (1989) 1887.

[6] H. Haug and S.W. Koch, Quantum Theory of the Optical and Electronic Properties of Semiconductors (World Scientific, Singapore 1990).

[7] G.P. Agrawal and N.K. Dutta, Long-Wavelength Semiconductor Lasers (Van Nostrand Reinhold, New York, 1986).

[8] K. Tai, T.R. Hayes, S.L. McCall and W.T. Tsang, Optical measurement of surface recombination in InGaAs quantum well mesa structures, Appl. Phys. Lett. 53 (1988) 302.

[9] O. Hess, Spatio-temporal dynamics of semiconductor lasers, Doctoral Thesis, Technische Universität Berlin, (Wissenschaft und Technik Verlag, Berlin, 1993).

[10] E. Schöll, D. Bimberg, H. Schumacher and P.T. Landsberg, IEEE J. Quantum Electron. 20 (1984) 394.

[11] M. Poliashenko, S.R. McKay and C.W. Smith, Chaotic dynamics due to the Shilnikov mechanism in two weakly nonlinear coupled oscillators, Proc. 18th Int. Conf. on Statistical Physics (Berlin, August 1992), book of abstracts (Berlin, 1992) p. 246;
M. Poliashenko and S.R. McKay, Phys. Rev. A 46 (1993) 5271.

[12] F. Schlögl, Z. Phys. 267 (1974) 77.

[13] F. Schlögl, Z. Phys. B 52 (1983) 51.

[14] W.H. Press, B.P. Flannery, S.A. Teukolsky and W.T. Vetterling, Numerical Recipes – The Art of Scientific Computing (FORTRAN Version) (Cambridge Univ. Press, Cambridge, 1989);
J.A. Fleck, Jr., Ultrashort-pulse generation by Q-switched lasers, Phys. Rev. B 1 (1970) 84–100;
I.S. Grieg and J.D. Morris, A Hopscotch method for the Korteweg-de Vries equation, J. Comput. Phys. 20 (1976) 60–84.

[15] P. Grassberger, Int. J. Phys. 25 (1993) 907.

[16] N.B. Abraham, A.M. Albano, A. Passamante and P.E. Rapp, eds. Measures of Complexity and Chaos, NATO ASI Series (Plenum, New York, 1989).

[17] F.T. Arecchi, Physica D 51 (1991) 450.